Journal of Solid State Chemistry **142,** 294–304 (1999)
Article ID jssc.1998.8034, available online at http://www.idealibrary.com on IDEAL®

New Structural and Electrical Data on Bi–Mo Mixed Oxides with a Structure Based on $[Bi_{12}O_{14}]_\infty$ Columns

Rose-Noëlle Vannier,[1] Francis Abraham, Guy Nowogrocki, and Gaëtan Mairesse

Laboratoire de Cristallochimie et Physicochimie du Solide, URA-CNRS 452, ENSCL, B.P. 108, 59652 Villeneuve d'Ascq Cedex, France

Received December 30, 1997; in revised form July 28, 1998; accepted September 23, 1998

We recently described a new family of oxide anion conductors with a structure based on $[Bi_{12}O_{14}]_\infty$ columns (*J. Solid. State Chem.* 122, 394 (1996)). The parent compound of this series can be formulated as $Bi_{26}Mo_{10}O_{69}$ and formation of a solid solution, in the Bi_2O_3–MoO_3 binary system, in the range $2.57 \leq Bi/Mo \leq 2.77$ was established. The stoichiometry of this series was questioned by R. Enjalbert *et al.* (*J. Solid State Chem.* 131, 236 (1997)), but confirmed by D. J. Buttrey *et al.* (*Mater. Res. Bull.* 32, 947 (1997)). The first part of this paper is devoted to a refutation criticisms by R. Enjalbert *et al.* In the second part, a comparison with other Bi_2O_3-based oxide anion conductors enables us to propose an iono-covalent description of this novel structure type, taking into account all the structural and electrical features, especially new neutron powder diffraction refinement and conductivity measurements under variable oxygen partial pressures.

Key Words: **bismuth molybdate; neutron powder diffraction; oxide ion conductor.**

INTRODUCTION

We recently described crystal structure and oxide anion conduction properties in a new family of Bi_2O_3-based mixed oxides (1). These compounds are built up from $[Bi_{12}O_{14}]_\infty$ columns containing typically Bi^{III}-oxygen surroundings, associated with additional extra Bi atoms between (Mo, V)O_4 tetrahedra (Fig. 1). The composition of the parent compound of this series can be written as $Bi_{26}Mo_{10}O_{69}$ and its structural characteristics extend within a continuous solid solution in the ternary Bi_2O_3–MoO_3–V_2O_5 system, especially in the Bi_2O_3–MoO_3 binary diagram within the range $2.57 \leq Bi/Mo \leq 2.77$. The symmetry is triclinic at room temperature; an increase of the bismuth content leads to the stabilization of a monoclinic phase at room temperature.

The structure of $Bi_{26}Mo_{10}O_{69}$ was determined from X-ray single crystal data in the apparent $P2/c$ space group and led to the following crystallographic formula: $[Bi_{12}O_{14}]_2(Bi)_2(MoO_4)_3$, i.e., $Bi_{26}Mo_{10}O_{68}$ instead of $Bi_{26}Mo_{10}O_{69}$, assuming Bi^{III} and Mo^{VI} valence states. As the existence of the Mo^V paramagnetic cation has been ruled out due to the absence of EPR signal, one additional oxygen may be present but was not revealed by X-ray crystal structure determination.

In the meantime D. J. Buttrey *et al.* (2) confirmed our structural study and our solid solution limits in the binary diagram. They refined the $Bi_{26}Mo_{10}O_{69}$ structure from powder neutron diffraction data and suggested the existence of an interstitial oxide to explain the oxygen stoichiometry, but their model led to a too short O–O bond length of 1.62 or 2.11 Å, depending on the constraints used in the refinement.

These basic structural features were also confirmed by R. Enjalbert *et al.* who published the structure of the isotype compounds $PbBi_{12}Mo_5O_{34}$ (3) and $Bi_{13}Mo_4VO_{34}$ (4), but they criticized our nonstoichiometry chemistry interpretation and proposed new domains of existence for such phases, based on strictly stoichiometric chemical formulations.

The first part of this paper is devoted to a refutation of the R. Enjalbert criticisms. In the second part, we present new experimental results, mainly a neutron diffraction refinement of the monoclinic $Bi/Mo = 2.75$ (upper limit of the binary solid solution), and the oxygen pressure dependence of electrical conductivity of $Bi_{26}Mo_{10}O_{69}$. By comparison with other Bi_2O_3-based oxide anion conductors, an iono-covalent description of this new monodimensional anionic conductor is proposed, taking into account all these experimental, structural, and electrical features.

EXPERIMENTAL

About 50 g of sample was prepared by solid state reaction from stoichiometric amounts of Bi_2O_3 and MoO_3 oxides in a covered gold crucible as previously described (1). A weight loss of less than 0.1% was observed at the end of the synthesis process. After checking the chemical purity by

[1]To whom correspondence should be addressed: E-mail: vannier@ensc-lille.fr.

0022-4596/99 $30.00

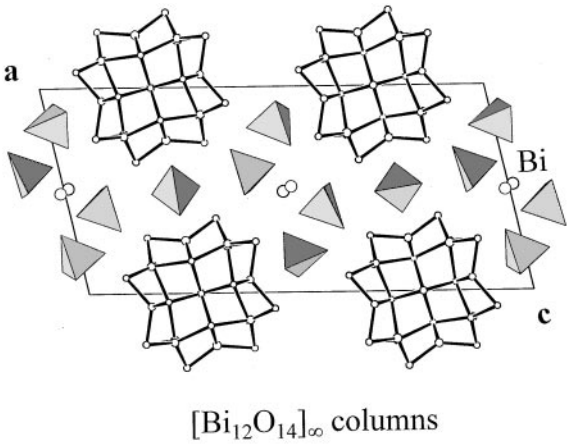

FIG. 1. (a, c) Projection of "$Bi_{26}Mo_{10}O_{68}$" structural model.

X-ray diffraction and X-ray fluorescence, neutron diffraction data were collected at room temperature on the high-resolution powder diffractometer D2B at the Institut Laue Langevin (ILL) at Grenoble. Approximately 40 g of compound were placed in a 15 mm-diameter cylindric vanadium can and data were collected in the range $0 \leq 2\theta \leq 161.95^\circ$ at a wavelength of $\lambda = 2.398$ Å using a graphite filter. The detector bank was stepped in 0.05° intervals in 2θ, and the resulting intensities were normalized with respect to detector efficiency and positional errors. Only data in the range $7 \leq 2\theta \leq 160^\circ$ were taken into account for the refinement.

Ionic transference number measurements have been performed using an oxygen-gas concentration cell.

CHEMICAL COMPOSITION AND OXYGEN STOICHIOMETRY

In their recent paper D. J. Buttrey *et al.* (2) found that $Bi_{26}Mo_{10}O_{69}$ "exhibits a solid solubility range of approximately $2.6 \leq Bi/Mo \leq 2.8$," in good agreement with our own proposed limits: $2.57 \leq Bi/Mo \leq 2.77$ (1).

Nevertheless R. Enjalbert *et al.* (4) disagreed with these results. According to these authors, and following their so-called "strict crystal chemistry rules," the various stoichiometries within the ternary Bi_2O_3–MoO_3–V_2O_5 should be limited to the compositions $1.75Bi_2O_3/1MoO_3$, $1.43Bi_2O_3/1MoO_3$, and $Bi_{26}Mo_8V_2O_{68}$. This triangular domain excludes our formulation, except for $Bi_{26}Mo_8V_2O_{68}$. To explain the discrepancies between our results and theirs, they proposed that some aluminum atoms could have substituted for Mo during our synthesis process using alumina crucible.

This last hypothesis can be readily discarded. Preparation of our powdered phases was performed either in alumina crucibles or in gold boats and led to the same compositions.

TABLE 1
Density Values Corresponding to the $Bi_{26}Mo_{10-y}Bi_yO_{69-1.5y}$ Solid Solution

Bi/Mo	d_{exp}	d_{th}[a]
2.60	7.54(2)	7.53 ($y = 0$)
2.70	7.57(2)	7.58 ($y = 0.27$)
2.75	7.63(2)	7.60 ($y = 0.40$)
2.77	7.61(2)	7.61 ($y = 0.46$)

[a] Assuming a $Bi_{26}Mo_{10-y}Bi_yO_{69-1.5y}$ unit per cell.

When preparing single crystals by melt cooling, gold boats were systematically used. Careful control of as-prepared samples by X-ray fluorescence analysis clearly indicated that, within our experimental conditions, no aluminum trace was detectable. The composition $Bi_{26}Mo_{9.33}Al_{0.67}O_{68}$, suggested by these authors, was synthesized for comparison and an aluminum signal was clearly obtained for this latter compound.

Moreover, during correction of this manuscript, a paper dealing with Bismuth based binary oxides was published (5). The authors prepared $Bi_{26}Mo_{10}O_{69}$ in sealed platinum tubes. They found a single phase and completely indexed its X-ray diagrams obtained from synchrotron radiation.

Furthermore, the measured densities (Table 1) obtained for compositions within the range $2.6 \leq Bi/Mo \leq 2.77$ agree very well with the hypothesis of bismuth substituting for molybdenum in $Bi_{26}Mo_{10}O_{69}$ to form a $Bi_{26}Mo_{10-y}Bi_yO_{69-1.5y}$ solid solution.

The conclusions of R. Enjalbert *et al.* (4) are in fact not based on experimental support but on two postulates that exclude the possibility of any defect chemistry in this new family of compounds:

> 1—the idea that extra Bi^{III} is present, substituting for Mo^{VI} is difficult to justify;
> 2—the $[MoO_4]$ tetrahedra cannot be affected by oxygen non-stoichiometry; such a hypothesis would be nonsense.

On the basis of the above, the only possible solid solutions must be built up from purely covalent chemical entities such as BiO_3E, BiO_4E (E = lone pair) and MO_4 ($M = Mo^{VI}$ and V^V). All the arguments developed by these authors are based on these so-called "strict crystal chemistry rules," where each chemical composition has to be perfectly stoichiometric.

Postulates 1 and 2 can both be disproved using well established recent experimental data:

1. Stabilization of the metastable γ polymorph of Bi_2O_3 can be achieved by addition of numerous oxides, leading to body-centered cubic phases related to the sillenite-type $Bi_{12}Si(or\ Ge)O_{20}$ crystal structure (6).

For a long time, the presence of Bi^V on tetrahedral sites was assumed to keep an exact number of oxygen atoms per

formula unit equal to 20. However, recent accurate investigations based on neutron and/or X-ray diffraction experiments clearly indicated the presence of Bi^{III} cations on the tetrahedral 2a crystallographic site. This Bi^{III} location generates oxygen vacancies on the anionic sites of the MO_4 tetrahedra, leading to the following formulations: $Bi_{12}(Bi_{0.67}Zn_{0.33})O_{19.33}$ and $Bi_{12}(BiFe)O_{19.5}$ (7), $Bi_{12}(Bi_{0.70}Co_{0.30})O_{19.35}$ (8), $Bi_{12}(Bi_{0.8-0.4y}Cd_y)O_{19.2+0.2y}$ (9) without requiring the presence of Bi^{V}.

2. In the BIMEVOX family of compounds, the solid solutions extend toward the Bi-rich part of the ternary diagrams Bi_2O_3–V_2O_5–ME_xO_z. This extension has been shown to be due to partial substitution of V^{v} by Bi^{III}, leading to the general formulation $Bi_2V_{1-x-y}ME_xBi_yO_z$ (10, 11).

3. Numerous compounds with scheelite-type structure exhibit oxide ion conduction due to oxygen non-stoichiometry. These compounds are mixed oxides with general composition ABO_4, and consist of A cation (Pb^{2+} in $PbWO_4$, Bi^{3+} in $BiVO_4$) ordered between BO_4 tetrahedra (12, 13). For example, doping of Pb with Sm in $PbWO_4$ forms $Pb_{1-x}Sm_xWO_{4+x/2}$ solid solutions, with x extending up to 0.15. Density measurements clearly indicate that interstitial oxygen ions are present in this scheelite-type phase and are responsible for the oxide anion conductivity (14).

To conclude this first part, and contrary to the assertions set out by R. Enjalbert *et al.*, the above examples clearly manifest the possible existence of oxygen under- and over-stoichiometry in structures containing Bi^{III} cations associated with MO_4 tetrahedral oxygen surroundings.

NEW EXPERIMENTAL RESULTS

1. Neutron Diffraction

In our first paper, the structure of $Bi_{26}Mo_{10}O_{69}$ had been determined from single crystal X-ray diffraction data (1). Although a good reliability factor was obtained at the end of the refinement: $R = 4.8\%$, high B values were observed for the oxygen atoms located in the molybdenum surroundings. R. Enjalbert *et al.* observed the same behavior (3, 4). The high B values could be an artifact resulting from poor quality of the absorption corrections applied, but we believe that they are more likely due to atomic displacements of the atoms which are correlated with some softness of the MoO part of the lattice which could favor the oxide ion mobility. In neutron diffraction, bismuth, molybdenum, and oxygen do not quite absorb; therefore, neutron diffraction would be a good technique for verifying this assumption.

From combined X-ray and neutron diffraction data, Buttrey *et al.* (2) confirmed our structural results, but they used a single thermal parameter for all the oxygen atoms. However, their valence bond sums and Madelung site potential calculations clearly revealed two kinds of oxygen: those located in the $[Bi_{12}O_{14}]_\infty$ columns, corresponding to short Bi–O distances with valence bond sums greater than 2, and those in the Molybdenum rich part, with valence bond sums lower than 2 and abnormally high Madelung potentials.

To satisfy the formal Bi^{III} and Mo^{VI} valence states and thereby the $Bi_{26}Mo_{10}O_{69}$ stoichiometry, these authors introduced an additional O(19) site with 25% occupancy in the surroundings of the isolated Bi(7) cation. However, this O(19) site led to abnormally short O(19)–O(15) bond lengths of 1.62 and 2.11 Å, depending on the refinement constraints used in the refinement. Furthermore, the refinement was performed in the $P2/c$ space group, although the actual symmetry was obviously triclinic.

In order to complete our structural study, neutron powder diffraction was performed on $Bi_{26}Mo_{10}O_{69}$ and on $Bi_{26}Mo_{9.6}Bi_{0.4}O_{68.4}$ (Bi/Mo = 2.75). The triclinic symmetry of $Bi_{26}Mo_{10}O_{69}$ was confirmed, but owing to the large number of parameters and their correlations, we did not manage to obtain satisfactory refinements in this case, and therefore results corresponding only to the monoclinic Bi/Mo = 2.75 composition are hereafter presented.

The Fullprof program (15) was used in the Rietveld refinement process.

1. In the first step, the $Bi_{26}Mo_{10}O_{68}$ crystallographic model obtained from single crystal X-ray diffraction in the $P2/c$ space group was used. A single thermal parameter was employed for all the oxygen atoms and led to a 3.59(9) $Å^2$ value with the following reliability factors: $R_p = 6.82\%$, $R_{wp} = 8.94\%$, $R_B = 13.52\%$, and $R_F = 11.39\%$. Oxygen bond valence sums (Table 2) are in accordance with the results of Buttrey *et al.* Two groups are clearly indicated: the O atoms in the Bismuth columns with a mean bond valence sum of 2.5 and those in the Molybdenum surroundings with a mean value of 1.9 (excepting O(11) and O(13), for which an

TABLE 2
Valence Bond Sums Obtained after a Refinement Using a Single Thermal Parameter for All the Oxygen Atoms

O in the $[Bi_{12}O_{14}]_\infty$ columns		O in the Mo–O surroundings	
O(1)	2.4(2)	O(9)	2.2(2)
O(2)	2.4(2)	O(10)	1.6(2)
O(3)	2.4(2)	O(11)	2.8(2)[a]
O(4)	2.5(2)	O(12)	1.6(2)
O(5)	2.6(2)	O(13)	2.9(3)[a]
O(6)	2.8(2)	O(14)	2.3(2)
O(7)	2.3(2)	O(15)	1.8(2)
O(8)	2.6(2)	O(16)	1.9(2)
		O(17)	1.7(1)
		O(18)	1.9(2)

Note. Bond valence sums are calculated using Brown and Altermatt R_0 tabulated values (18).

[a] Overestimated valence sums are obtained for these oxygen due to too short Mo–O bond-lengths: Mo(1)–O(11) = 1.59 Å and Mo(2)–O(13) = 1.57 Å.

erroneous sum is observed due to the too small Mo–O bond lengths (see below)).

2. Therefore, in the second step, two kinds of thermal parameters were used for O atoms: one for those belonging to the $[Bi_{12}O_{14}]_\infty$ columns and the other for those in the Molybdenum surroundings. A value of 0.45(7) Å^2 was obtained for the first group and 8.6(2) Å^2 was obtained for the second. The reliability factors were dramatically improved: $R_p = 4.96\%$, $R_{wp} = 6.41\%$, $R_B = 9.00\%$, and $R_F = 8.36\%$. Clearly two types of oxide ion occur in these compounds.

3. In the third step, thermal parameters of the oxygen atoms in the molybdenum surrounding were allowed to vary independently; to satisfy the chemical composition $Bi_{26}Mo_{9.6}Bi_{0.4}O_{68.4}$, 0.4 Bi was distributed among the three Molybdenum sites.

At that point, the inherent limitations of neutron powder diffraction are reached, due to limited resolution of neutrons, limited number of diffraction peaks, and overlapping; we did not manage to localize the 0.4 missing oxygen by Fourier synthesis.

2. A Geometrical Comparison with the Fluorite Structure

To identify structural relationships between bismuth molybdate crystal structures and catalytic properties, D. J. Buttrey *et al.* examined the structural features of numerous phases, describing them as fluorite-derived compounds: $\alpha Bi_2Mo_3O_{12}$, β $Bi_2Mo_2O_9$, $\gamma(L)$-Bi_2MoO_6 (16) and $\gamma(H)$-Bi_2MoO_6 (17) but they considered $Bi_{26}Mo_{10}O_{69}$ as an intergrowth between a fluorite motif and a new monoclinic variation of the cationic arrangement, which is, in fact, a strongly distorted fluorite-like band.

Using their structural approach, a projection of the $Bi_{26}Mo_{10}O_{68}$ model in the (a, c) plane is shown in Fig. 2. Bi and Mo cations are indistinguishably represented either by a square (at the $y \approx 0$ level), or by a triangle ($y \approx 1/2$). Oxygen atoms within the $0 \leq y \leq 0.5$ half unitcell are symbolized by small circles. Clearly, the cationic arrangement is related to a distorted fluorite-like fcc lattice where oxygen atoms occupy tetrahedral sites. In their recent paper, C. D. Ling *et al.* (5) provided an equivalent vectorial relationship between the $Bi_{26}Mo_{10}O_{69}$ unit cell and that of the fluorite. Two unoccupied symmetry related Oxygen sites are observed at about $x \approx 0.45$ and $z \approx 0.15$.

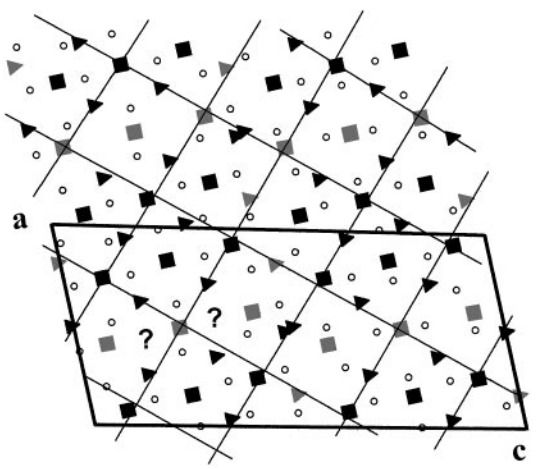

FIG. 2. (a, c) Projection of "$Bi_{26}Mo_{10}O_{68}$": Bi and Mo are represented by ■ for atoms in $y \approx 0$ and ▲ for atoms in $y \approx 0.5$. ○ represents oxygen atoms with $0 \leq y \leq 0.5$.

Thus, an O(19) additional oxygen position with 10% occupancy was introduced in order to respect the formal chemical composition and mainly to check the geometrical compatibility of this site with its occupation by an O atom.

With this small amount of this extra oxygen, a value of 2.55 Å with a standard error of 0.05 was introduced for O(19)–O(12), O(19)–O(17), O(19)–O(17)^e distances. As a matter of fact, introducing or omitting this extra oxygen does not effectively change the accuracy of the refinement (Table 4).

In the first step the Mo–O distances were unconstrained. As the refinement led to too short Mo(1)–O(11), Mo(2)–O(13), and Mo(2)–O(14) bond lengths of 1.58(2), 1.69(3), and 1.66(2) Å, respectively, and therefore to erroneous valence sums, in the second step a value of 1.75 Å with a standard error of 0.02 for these bond lengths was introduced in the refinement. It led to slightly modified values of 1.65(2), 1.71(3), and 1.69(2) Å in the range of the smallest Mo–O distances previously obtained, 1.68(4) Å (3) and 1.70 Å(2), and to a more realistic O(11) valence sum of 2.5(2) instead of 2.8(2).

Final results are reported in Tables 3 and 4. The final calculated pattern is compared with the experimental one in Fig. 3. A good concordance is observed, the calculated distances confirm the existence of some space for additional O atom and answer the statement of R. Enjalbert *et al.* who claimed that "it is rather hard to see where any additional oxygen could be added!"

An additional remark can be made. This relationship between the geometric arrangement of atoms in the structure and that of atoms in fluorite does not mean that the description of this structure using the fluorite model is the most relevant one. As pointed out by C. D. Ling (5), "the $Bi_{26}Mo_{10}O_{69}$ average structure clearly appears to have moved too far from that prototype to be usefully described as a modulation thereof."

3. Conduction Properties

3a. Ionic conductivity. In our first paper, conductivity measurements revealed that these materials were good ionic conductors (1). To complete this study, the ionic transference number of oxide ion was measured on the undoped material and on the Bi/Mo = 2.75 composition using an air/pure oxygen concentration cell. Values close to unity

TABLE 3
Positional Parameters Corresponding to $Bi_{26}Mo_{9.6}Bi_{0.4}O_{68.4}$

Atom	Site	Occ.	x	y	z	B (Å^2)
Bi(1)	4g	1	0.0409(8)	0.416(2)	0.3261(4)	1.15(5)
Bi(2)	4g	1	0.1584(7)	0.920(2)	0.2456(3)	1.15(5)
Bi(3)	4g	1	0.2483(6)	0.008(2)	0.4013(3)	1.15(5)
Bi(4)	4g	1	0.3607(7)	0.502(2)	0.3241(3)	1.15(5)
Bi(5)	4g	1	0.2698(6)	0.501(2)	0.1597(3)	1.15(5)
Bi(6)	4g	1	0.0761(6)	0.004(2)	0.0908(3)	1.15(5)
Bi(7)	4g	0.5	0.522(2)	0.536(4)	0.009(1)	2.9(5)
Mo(1)/Bi	4g	0.96/0.04	0.4162(7)	−0.007(2)	0.0782(4)	0.8(3)
Mo(2)/Bi	4g	0.96/0.04	0.8329(8)	0.512(2)	0.0105(4)	1.8(3)
Mo(3)/Bi	2f	0.48/0.02	$\frac{1}{2}$	0.006(3)	$\frac{1}{4}$	1.5(4)
O(1)	2e	1	0	0.713(3)	$\frac{1}{4}$	0.62(7)
O(2)	4g	1	0.1438(9)	0.258(2)	0.1584(5)	0.62(7)
O(3)	4g	1	0.1264(9)	0.755(2)	0.1539(5)	0.62(7)
O(4)	4g	1	0.237(1)	0.766(2)	0.3368(5)	0.62(7)
O(5)	4g	1	0.2529(9)	0.591(2)	0.2424(5)	0.62(7)
O(6)	4g	1	0.0610(9)	0.068(2)	0.3670(4)	0.62(7)
O(7)	2e	1	0	0.222(3)	$\frac{1}{4}$	0.62(7)
O(8)	4g	1	0.235(1)	0.265(2)	0.3362(5)	0.62(7)
O(9)	4g	1	0.514(2)	−0.254(4)	0.0851(8)	8.6(6)
O(10)	4g	1	0.384(2)	0.106(4)	0.0100(8)	9.9(7)
O(11)	4g	1	0.304(2)	−0.009(4)	0.1080(7)	9.8(5)
O(12)	4g	1	0.531(2)	0.216(4)	0.0967(9)	10.4(7)
O(13)	4g	1	0.932(2)	0.293(3)	0.0284(8)	11.0(7)
O(14)	4g	1	0.799(2)	0.561(3)	−0.0583(5)	6.6(5)
O(15)	4g	1	0.885(2)	0.757(3)	0.0463(7)	6.7(5)
O(16)	4g	1	0.708(2)	0.423(3)	0.0377(7)	7.0(5)
O(17)	4g	1	0.375(2)	0.172(3)	0.2423(8)	5.3(5)
O(18)	4g	1	0.478(2)	−0.167(4)	0.1905(8)	10.6(7)
O(19)	**4g**	**0.1**	**0.485(6)**	**0.39(2)**	**0.182(2)**	**10(1)**

Note. $a = 11.7525(2)$ Å, $b = 5.8005(1)$ Å, $c = 24.8024(4)$ Å, $\beta = 102.867(1)^\circ$. $R_p = 4.76\%$, $R_{wp} = 6.17\%$, ($R_E = 1.79\%$). $R_B = 8.58\%$, $R_F = 8.01\%$. No. of reflections: 971.

were systematically observed over the explored temperature range (up to about 800°C). To confirm that these materials were pure oxide anion conductors, conductivity measurements were performed on $Bi_{26}Mo_{10}O_{69}$ under oxygen partial pressure up to 790°C. The results are reported in Fig. 4. Up to 719°C no deviation is observed. At 740°C, even if we are at the detection limit, a very small increase of the conductivity at low partial pressure is to be noticed, which indicates a small degree of *n*-type electronic semiconductivity contribution at this temperature.

These materials can thereby be considered as very good oxide ion conductors with negligible electronic contribution up to about 750°C within the oxygen partial pressure range investigated.

3b. The modulated background: A further experimental signature of oxygen diffusion. Fast oxygen diffusion can lead to important structural disorder (19) and in this case the long-range order included in the Bragg reflections is replaced by short-range order, characterized by atom pairs merged in a quasi-liquid-like structure. This local atomic order has no effect on the intensities of the Bragg reflections but influences the elastic scattering merely by modulating the background.

The background intensity of a neutron diffractogram may be written as the sum of three components (20),

$$I = I_{inc} + I_{TDS} + I_{EDS},$$

where

— I_{inc} is the coherent scattering intensity which is isotropic. It leads to a constant contribution to the background.

— I_{TDS} is the thermal diffuse inelastic scattering (TDS) intensity, which can be calculated in a first approximation for a given θ by

$$I_{TDS} = \sum (1 - \exp(-2B_i^{th} \sin^2\theta/\lambda^2))b_i^2,$$

with b_i the coherent scattering length of the atom i, and B_i^{th} the corresponding Debye-Waller factor.

— I_{EDS} is the elastic diffuse scattering which originates from a local static structural disorder. In a first approximation, it can be expressed by a similar formalism where a pseudo-B_i^{dis} Debye-Waller factor appears:

$$I_{EDS} = \sum (1 - \exp(-2B_i^{dis} \sin^2\theta/\lambda^2))b_i^2.$$

The thermal B factor obtained from structural refinements of the Bragg peak intensities is the sum of these two contributions: $B = B_i^{th} + B_i^{dis}$.

In our case, the small thermal parameter of 0.62(7) Å^2 obtained for O atoms in the $[Bi_{12}O_{14}]_\infty$ columns clearly indicates that these atoms are not affected by diffusion motions; we can therefore consider a value of $B^{th} = 0.62(7)$ Å^2 for an O atom. By contrast, O atoms in the molybdenum surroundings are merely characterized by diffusive motion with high B values.

When the static structural disorder is too important, I_{EDS} can therefore be expressed using the Debye formula:

$$I_{EDS} = 1 + 1/N_{(\text{Nb of pair of atoms})} \sum \sin(Q.r_{ij})/(Q.r_{ij})$$
$$\text{with } Q = 4\pi \sin\theta/\lambda.$$

The Debye formula exhibits a first marked maximum for $Q_{max} = (2\pi \times 1.23)/d_m$ where d_m is a preferred pair distance.

A close-up of the background corresponding to the Bi/Mo = 2.75 neutron diffraction pattern is shown in Fig. 5. Although a large number of diffraction lines overlap, the modulation is clearly noticeable.

The background intensity corresponding to Bi/Mo = 2.75 versus Q is reported in Fig. 6. A maximum is observed

TABLE 4a
Bond Lenghts (in Å) Corresponding to $Bi_{26}Mo_{9.6}Bi_{0.4}O_{68.4}$

Refinement	Without O(19)	With O(19)	With Mo–O constraints
Bi(1)–			
O(1)	2.52(2)	2.52(2)	2.52(2)
O(2)[a]	2.46(2)	2.47(2)	2.46(2)
O(3)[a]	2.91(2)	2.90(2)	2.90(2)
O(4)	3.04(2)	3.04(2)	3.03(2)
O(6)	2.25(2)	2.25(2)	2.25(2)
O(7)	2.15(2)	2.15(2)	2.16(2)
O(8)	2.40(2)	2.40(2)	2.41(2)
Valence sum	*2.8(2)*	*2.8(2)*	*2.8(2)*
Bi(4)–			
O(4)	2.18(2)	*2.19(2)*	*2.19(2)*
O(5)	2.20(2)	*2.20(2)*	2.20(2)
O(8)	2.09(2)	*2.09(2)*	2.09(2)
O(9)[h]	2.77(3)	*2.78(3)*	2.79(3)
O(12)[e]	2.64(3)	*2.66(3)*	2.66(3)
O(17)	2.82(2)	*2.82(2)*	2.82(2)
O(18)[h]	2.77(3)	*2.77(3)*	2.78(3)
O(19)[e]		*1.96(7)*	1.97(7)
Valence sum	*3.2(2)*	*3.3(2)*	*3.3(2)*
Bi(7)–			
O(9)[b]	2.28(4)	2.27(4)	2.27(3)
O(9)[l]	2.81(4)	2.81(4)	2.80(3)
O(10)	2.96(3)	2.99(3)	2.98(3)
O(10)[i]	2.44(3)	2.44(3)	2.44(3)
O(12)	2.87(4)	2.86(4)	2.85(4)
O(12)[i]	2.95(4)	2.93(4)	2.93(4)
O(16)	2.26(3)	2.26(3)	2.25(3)
O(16)[i]	2.69(3)	2.70(3)	2.70(3)
Valence sum	*2.3(3)*	*2.3(3)*	*2.3(2)*
Mo(3)/Bi–			
O(17)	1.72(2)	1.74(2)	1.73(2)
O(18)	1.75(2)	1.76(3)	1.76(3)
O(19)		2.76(6)	2.75(6)
Valence sum	*6.4(5)*	*6.1(5)*	*6.2(5)*

Refinement	Without O(19)	With O(19)	With Mo–O constraints
Bi(2)–			
O(1)	2.24(2)	2.24(2)	2.24(2)
O(2)[b]	2.89(2)	2.89(2)	2.90(2)
O(3)	2.42(2)	2.42(2)	2.42(2)
O(4)	2.42(2)	2.41(2)	2.41(2)
O(5)	2.22(2)	2.21(2)	2.21(2)
O(7)[b]	2.58(2)	2.58(2)	2.58(2)
O(8)[b]	2.99(2)	2.99(2)	2.99(2)
O(17)[b]	2.96(2)	2.95(2)	2.95(2)
Valence sum	*2.8(2)*	*2.8(2)*	*2.8(2)*
Bi(5)–			
O(2)	2.04(2)	2.04(2)	2.04(2)
O(3)	2.22(2)	2.22(2)	2.22(2)
O(5)	2.17(2)	2.17(2)	2.17(2)
O(11)	3.34(3)	3.32(3)	3.29(3)
O(11)[b]	3.17(3)	3.19(3)	3.18(3)
O(14)[i]	2.50(2)	2.51(2)	2.49(2)
O(17)	2.87(2)	2.87(2)	2.87(2)
O(18)[b]	3.05(3)	3.08(3)	3.07(3)
O(19)[e]		2.56(7)	2.56(3)
Valence sum	*3.3(2)*	*3.3(2)*	*3.3(2)*
Mo(1)/Bi–			
O(9)	1.83(3)	1.82(3)	1.82(3)
O(10)	1.78(3)	1.78(3)	1.77(2)
O(11)	1.59(2)	1.58(2)	*1.65(2)**
O(12)	1.85(3)	1.85(3)	1.85(3)
O(18)	2.90(3)	2.87(3)	2.87(3)
O(19)		3.43(6)	3.40(6)
Valence sum	*6.2(5)*	*6.3(5)*	*5.9(4)*

Refinement	Without O(19)	With O(19)	With Mo–O constraints
Bi(3)–			
O(4)[d]	2.11(2)	2.11(2)	2.11(2)
O(6)	2.20(2)	2.21(2)	2.20(2)
O(8)	2.18(2)	2.18(2)	2.18(2)
O(9)[e]	3.14(3)	3.13(3)	3.13(3)
O(10)[f]	2.90(2)	2.88(2)	2.89(2)
O(12)[e]	2.86(3)	2.86(3)	2.85(3)
O(13)[e]	3.45(3)	3.45(3)	3.45(2)
O(15)[g]	2.68(2)	2.68(2)	2.68(2)
O(16)[e]	2.81(2)	2.82(2)	2.83(2)
Valence sum	*3.1(2)*	*3.2(2)*	*3.2(2)*
Bi(6)–			
O(2)	2.24(2)	2.24(2)	2.24(2)
O(3)[j]	2.11(2)	2.11(2)	2.11(2)
O(6)[a]	2.14(2)	2.14(2)	2.14(2)
O(11)	2.65(2)	2.66(2)	2.62(2)
O(13)[k]	2.66(3)	2.65(2)	2.63(2)
O(13)[l]	3.42(3)	3.41(3)	3.40(2)
O(14)[i]	3.12(2)	3.12(6)	3.11(2)
O(15)[m]	2.68(2)	2.67(2)	2.68(2)
Valence sum	*3.2(2)*	*3.3(2)*	*3.3(2)*
Mo(2)/Bi–			
O(10)[i]	3.33(3)	3.33(3)	3.32(3)
O(13)	1.69(3)	1.69(3)	*1.71(3)**
O(13)[n]	3.33(3)	3.33(3)	3.32(3)
O(14)	1.66(2)	1.66(2)	*1.69(2)**
O(15)	1.73(2)	1.73(2)	1.72(2)
O(16)	1.83(2)	1.83(2)	1.82(2)
Valence sum	*6.6(5)*	*6.7(5)*	*6.5(4)*

Note. Bond valence are calculated using Brown and Altermatt R_0 tabulated values (18).
*Constrained.
[a] $-x, y, \frac{1}{2}-z$.
[b] $x, 1+y, z$.
[c] $-x, 1+y, \frac{1}{2}-z$.
[d] $x, y-1, z$.
[e] $1-x, y, \frac{1}{2}-z$.
[f] $x, -y, \frac{1}{2}+z$.
[g] $1-x, y-1, \frac{1}{2}-z$.
[h] $1-x, 1+y, \frac{1}{2}-z$.
[i] $1-x, 1-y, -z$.
[j] $x, y-1, z$.
[k] $1-x, y, z$.
[l] $1-x, -y, -z$.
[m] $x-1, y-1, z$.
[n] $2-x, 1-y, -z$.

TABLE 4b
O–O Distances in Å

Refinement	Without O(19)	With O(19)	With Mo–O constraints	Refinement	Without O(19)	With O(19)	With Mo–O constraints	Refinement	Without O(19)	With O(19)	With Mo–O constraints
O(1)–O(3)	3.08(2)	3.09(2)	3.09(2)	O(2)–O(3)[j]	2.92(2)	2.92(2)	2.92(2)	O(3)–O(5)	2.54(2)	2.55(2)	2.55(2)
O(1)–O(4)	3.14(2)	3.13(2)	3.13(2)	O(2)–O(3)	2.89(2)	2.89(2)	2.89(2)	O(3)–O(6)[c]	2.81(2)	2.81(2)	2.81(2)
O(1)–O(5)	3.10(2)	3.10(2)	3.10(2)	O(2)–O(5)	2.92(2)	2.92(2)	2.92(2)	O(3)–O(11)[b]	2.95(3)	2.97(3)	2.93(3)
O(1)–O(7)	2.85(3)	2.85(3)	2.84(3)	O(2)–O(6)[a]	2.60(2)	2.59(2)	2.59(2)	O(3)–O(14)[i]	3.28(2)	3.27(2)	3.26(2)
O(1)–O(7)[b]	2.95(3)	2.95(3)	2.96(3)	O(2)–O(7)	3.12(2)	3.12(2)	3.13(2)	O(3)–O(15)[k]	3.43(2)	3.42(2)	3.43(2)
Valence sum	*2.1(2)*	*2.1(2)*	*2.1(2)*	O(2)–O(11)	2.99(3)	2.98(3)	2.93(3)	Valence sum	*2.4(2)*	*2.4(2)*	*2.4(2)*
O(4)–O(5)	2.59(2)	2.60(2)	2.60(2)	O(2)–O(14)[i]	2.93(2)	2.93(2)	2.91(2)	O(6)–O(7)	2.97(2)	2.97(2)	2.97(2)
O(4)–O(6)[b]	2.93(2)	2.93(2)	2.93(2)	O(2)–O(17)	3.07(2)	3.07(2)	3.07(2)	O(6)–O(8)	2.60(2)	2.60(2)	2.60(2)
O(4)–O(8)	2.90(2)	2.91(2)	2.91(2)	Valence sum	*2.5(2)*	*2.5(2)*	*2.5(2)*	O(6)–O(13)[e]	2.90(3)	2.89(3)	2.89(3)
O(4)–O(8)[b]	2.90(2)	2.89(2)	2.89(2)	O(5)–O(8)	3.04(2)	3.04(2)	3.04(2)	O(6)–O(15)[g]	2.76(2)	2.76(2)	2.77(2)
O(4)–O(9)[h]	3.12(3)	3.13(3)	3.14(3)	O(5)–O(17)	2.83(2)	2.82(2)	2.83(2)	Valence sum	*2.5(2)*	*2.5(2)*	*2.5(2)*
Valence sum	*2.3(2)*	*2.4(2)*	*2.4(2)*	O(5)–O(18)[b]	3.44(3)	3.49(3)	3.48(3)	O(7)–O(8)	3.10(2)	3.10(2)	3.10(2)
O(9)–O(10)	2.99(3)	2.98(3)	2.99(3)	O(5)–O(19)[e]		3.41(6)	3.44(6)	Valence sum	*2.4(2)*	*2.4(2)*	*2.4(2)*
O(9)–O(10)[l]	3.01(3)	3.00(3)	3.00(3)	Valence sum	*2.5(2)*	*2.5(2)*	*2.5(2)*	O(8)–O(12)[e]	2.89(3)	2.90(3)	2.89(3)
O(9)–O(11)	2.95(3)	2.96(3)	3.01(3)	O(10)–O(10)[l]	3.12(3)	3.12(3)	3.13(3)	O(8)–O(16)[e]	3.18(2)	3.18(2)	3.19(2)
O(9)–O(12)[j]	3.08(3)	3.09(3)	3.08(3)	O(10)–O(11)	2.84(3)	2.83(3)	2.87(3)	O(8)–O(17)	3.19(2)	3.18(2)	3.18(2)
O(9)–O(12)	2.75(3)	2.75(3)	2.75(3)	O(10)–O(12)	2.53(3)	2.53(3)	2.52(3)	Valence sum	*2.5(2)*	*2.5(2)*	*2.5(2)*
O(9)–O(16)[j]	3.37(3)	3.37(3)	3.36(3)	O(10)–O(14)[i]	3.30(3)	3.32(3)	3.31(3)	O(11)–O(12)	3.01(3)	3.00(3)	3.04(3)
O(9)–O(18)	2.80(3)	2.78(3)	2.79(3)	O(10)–O(15)[i]	3.27(3)	3.27(3)	3.26(3)	O(11)–O(14)[i]	3.05(3)	3.04(3)	3.02(3)
O(9)–O(19)[j]		3.26(6)	3.26(6)	O(10)–O(16)[i]	3.38(3)	3.37(3)	3.38(3)	O(11)–O(17)	3.45(3)	3.45(3)	3.41(3)
Valence sum	*2.0(2)*	*2.0(2)*	*2.0(2)*	O(10)–O(16)[i]	3.09(3)	3.09(3)	3.07(3)	O(11)–O(18)	2.73(3)	2.71(3)	2.71(3)
O(12)–O(16)	3.06(3)	3.06(3)	3.04(3)	Valence sum	*2.0(2)*	*2.0(2)*	*2.0(2)*	O(11)–O(19)		3.42(6)	3.38(7)
O(12)–O(18)	3.40(3)	3.37(3)	3.38(3)	O(13)–O(13)[n]	3.36(3)	3.36(3)	3.37(3)	Valence sum	*2.8(2)*	*2.8(2)*	*2.5(2)*
O(12)–O(19)		2.52(6)	2.50(6)	O(13)–O(14)	2.79(3)	2.79(3)	2.82(3)	O(14)–O(15)	2.80(3)	2.80(3)	2.81(3)
Valence sum	*1.8(2)*	*1.8(2)*	*1.8(2)*	O(13)–O(14)[n]	3.22(3)	3.20(3)	3.20(3)	O(14)–O(16)	2.92(2)	2.92(2)	2.93(2)
O(17)–O(17)[e]	2.86(3)	2.89(3)	2.88(3)	O(13)–O(15)[j]	3.21(3)	3.21(3)	3.20(3)	Valence sum	*2.5(2)*	*2.5(2)*	*2.3(2)*
O(17)–O(18)	2.76(3)	2.77(3)	2.77(3)	O(13)–O(15)	2.79(3)	2.79(3)	2.80(3)	O(15)–O(16)	2.84(3)	2.83(3)	2.82(3)
O(17)–O(18)[e]	2.90(3)	2.89(3)	2.89(3)	O(13)–O(15)[n]	3.16(3)	3.16(3)	3.15(3)	Valence sum	*2.2(2)*	*2.2(2)*	*2.2(2)*
O(17)–O(19)		2.51(6)	2.51(6)	O(13)–O(16)	2.76(3)	2.77(3)	2.79(3)	O(18)–O(18)[e]	2.81(3)	2.88(3)	2.88(3)
O(17)–O(19)[e]		2.52(6)	2.52(6)	Valence sum	*2.2(2)*	*2.2(2)*	*2.2(2)*	O(18)–O(19)[j]		2.58(7)	2.61(7)
Valence sum	*2.2(2)*	*2.2(2)*	*2.2(2)*	O(19)–O(19)[e]		3.25(7)	3.30(7)	O(18)–O(19)		3.24(7)	3.21(7)
				Valence sum		*2.1(4)*	*2.1(4)*	Valence sum	*1.98(2)*	*2.04(2)*	*2.04(2)*

[a] $-x, y, \frac{1}{2}-z$.
[b] $x, 1+y, z$.
[c] $-x, 1+y, \frac{1}{2}-z$.
[d] $x, y-1, z$.
[e] $1-x, y, \frac{1}{2}-z$.
[f] $x, -y, \frac{1}{2}+z$.
[g] $1-x, y-1, \frac{1}{2}-z$.
[h] $1-x, 1+y, \frac{1}{2}-z$.
[i] $1-x, 1-y, -z$.
[j] $x, y-1, z$.
[k] $1-x, y, z$.
[l] $1-x, -y, -z$.
[m] $x-1, y-1, z$.
[n] $2-x, 1-y, -z$.

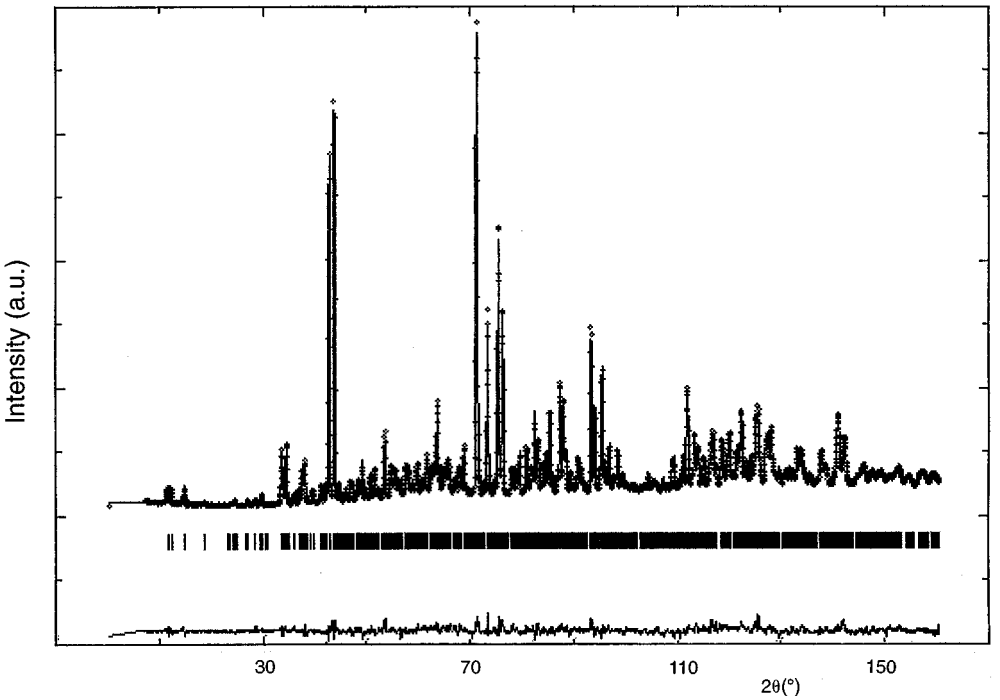

FIG. 3. $Bi_{26}Mo_{9.6}Bi_{0.4}O_{68.4}$ calculated neutron diffraction pattern compared to the experimental one.

for $Q_{max} = 2.75$ Å, leading to a preferred pair distance of 2.8 Å. This value is characteristic of an O–O distance and is a further proof of fast oxygen diffusion in this new family of materials.

DISCUSSION

The main bond lengths and valence sums are reported in Tables 3 and 4 and in Fig. 7. The following comments can be made:

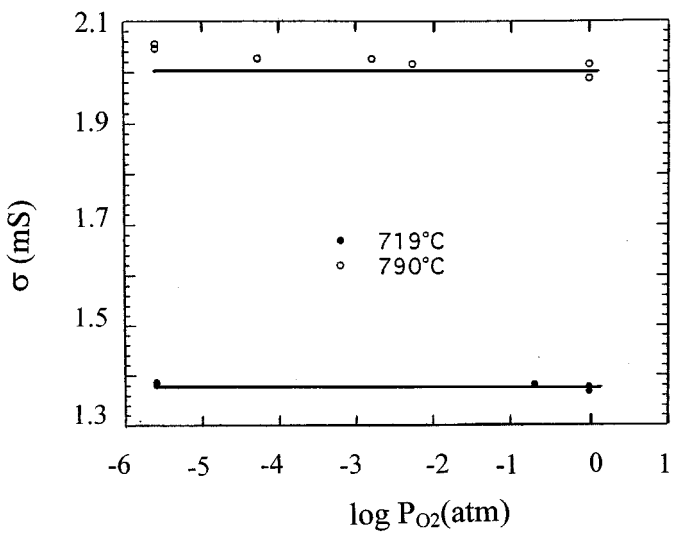

FIG. 4. Conductivity versus oxygen partial pressure.

1. Introduction of O(19) atom and Mo–O constraints do not modify the results.

2. The surroundings of the extra O(19) atom exhibit no physically unacceptable characteristics. They give rise to a statistical octahedral/tetrahedral environment for Mo(3). Therefore, unlike the affirmation of R. Enjalbert *et al.*, there remains space to insert additional oxygen corresponding to the nonstoichiometric formulation.

3. Bismuth and molybdenum valence states of III and VI, respectively, are confirmed.

4. Clearly two groups of oxygen atoms are evidenced. The iono-covalent character of this material is confirmed: high thermal parameters are obtained for oxygen in the molybdenum area, including O(19), and small values for those in the bismuth columns. This behavior cannot be the result of erroneous absorption corrections in the X-ray study and evidently is a basic structural characteristic of this series of compounds.

The structure of these materials has to be described as an iono-covalent one combining covalent $[Bi_{12}O_{14}]_\infty$ columns, characterized by short Bi–O bond lengths, small thermal parameters, and overbonded oxygen atoms (with bond sum higher than 2) connected with an Mo–O area in which the displacements of the atoms display unusual high values, likely correlated with softness of this part of the lattice, which favors the oxide ion mobility.

The combination of an ionic part exhibiting defect oxygen stoichiometry and/or structural disorder responsible for oxygen diffusion, and a covalent part which is the skeleton

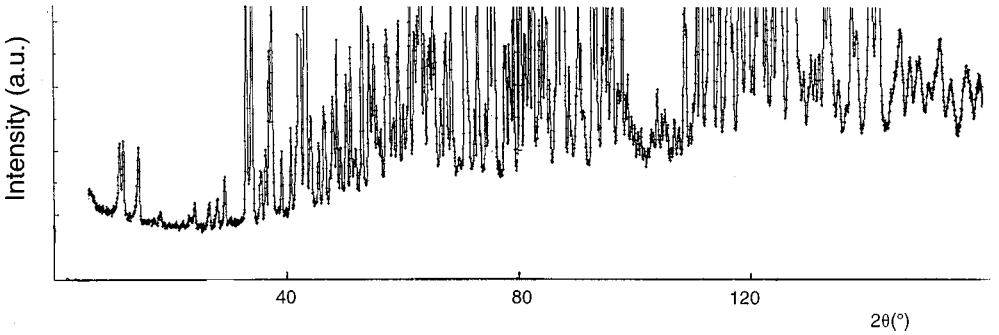

FIG. 5. Zoom on $Bi_{26}Mo_{9.6}Bi_{0.4}O_{68.4}$ neutron diffraction pattern: a modulated background is evidenced.

of the structure, is a classical observation in several bismuth-oxide-based anionic conductors.

Indeed, Bi_2O_3-based oxide anionic conductors can be classified according to the dimensionality of this property:

— *Three-dimensional oxide ion conductors* are those related to the fluorite type structure δBi_2O_3 stabilized by numerous appropriate dopants. The choice of cations which can be used is very large, going from divalent up to hexavalent elements (21, 22).

Another example of such three dimensional oxide anion conductor is encountered with the so-called β-type phase of the bismuth–lead mixed oxide with α-anti AgI crystal structure. Similar structural β-type compounds exist with Cd, *Ln* (*Ln* = Gd, Dy, Tm) and Sb as dopants (23–25).

— *Two-dimensional oxide ion conductors* have two classes of compounds that correspond to this type. From an historical view point, the first documented one was the rhombohedral type structure, obtained with alkaline-earth cations (26–28). The second is the Aurivillius-type $(Bi_2O_2)(A_{n-1}B_nO_x)$ family, encompassing intrinsic oxygen ion conductors (BIMEVOX) (10, 21, 29–34) and extrinsic oxygen ion conductors (doped $n = 1$ Bi_2WO_6 with Nb or Ta (35–36), $n = 2$ (Bi_2O_2) $[Ca_{1-x}Na_x(Nb)_2O_{7-x/2}]$, with x in the range $0 \leq x \leq 1$ (37), $n = 3$ $(Bi_2O_2)[Sr_2(M^V_2M'^{III})O_{9.5}]$ with M^V = Nb, Ta and M'^{III} = Al, Ga (38)…). In both rhombohedral and Aurivillius-type materials, covalent two-dimensional blocks containing short Bi–O distances alternate with more ionic sheets, and the nonbonding electronic $6s^2$ lone pairs of the Bi^{III} cations are oriented toward this

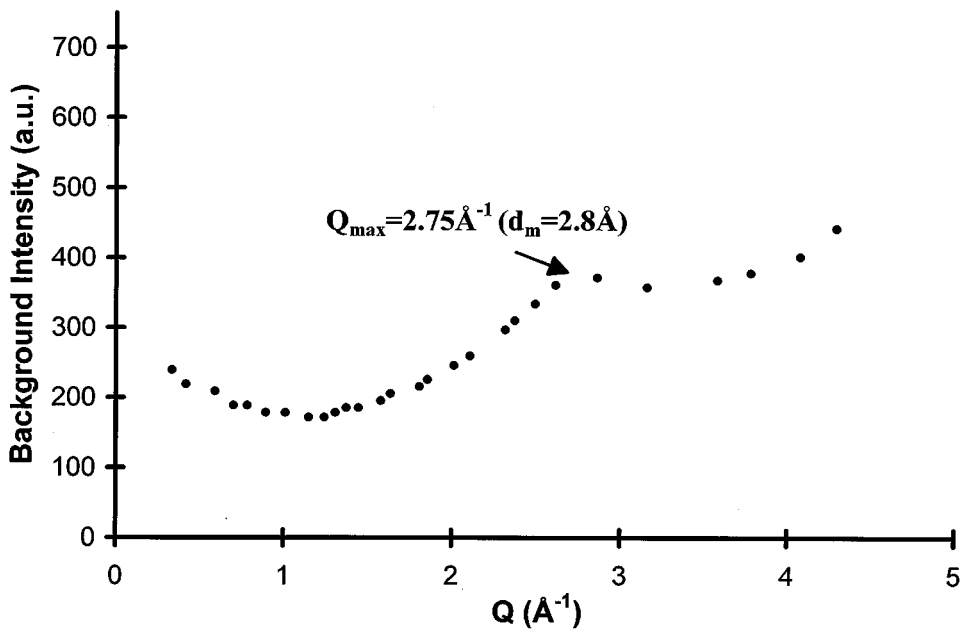

FIG. 6. Background intensity corresponding to $Bi_{26}Mo_{9.6}Bi_{0.4}O_{68.4}$ neutron diffraction pattern versus $Q = 4\pi \sin\theta/\lambda$.

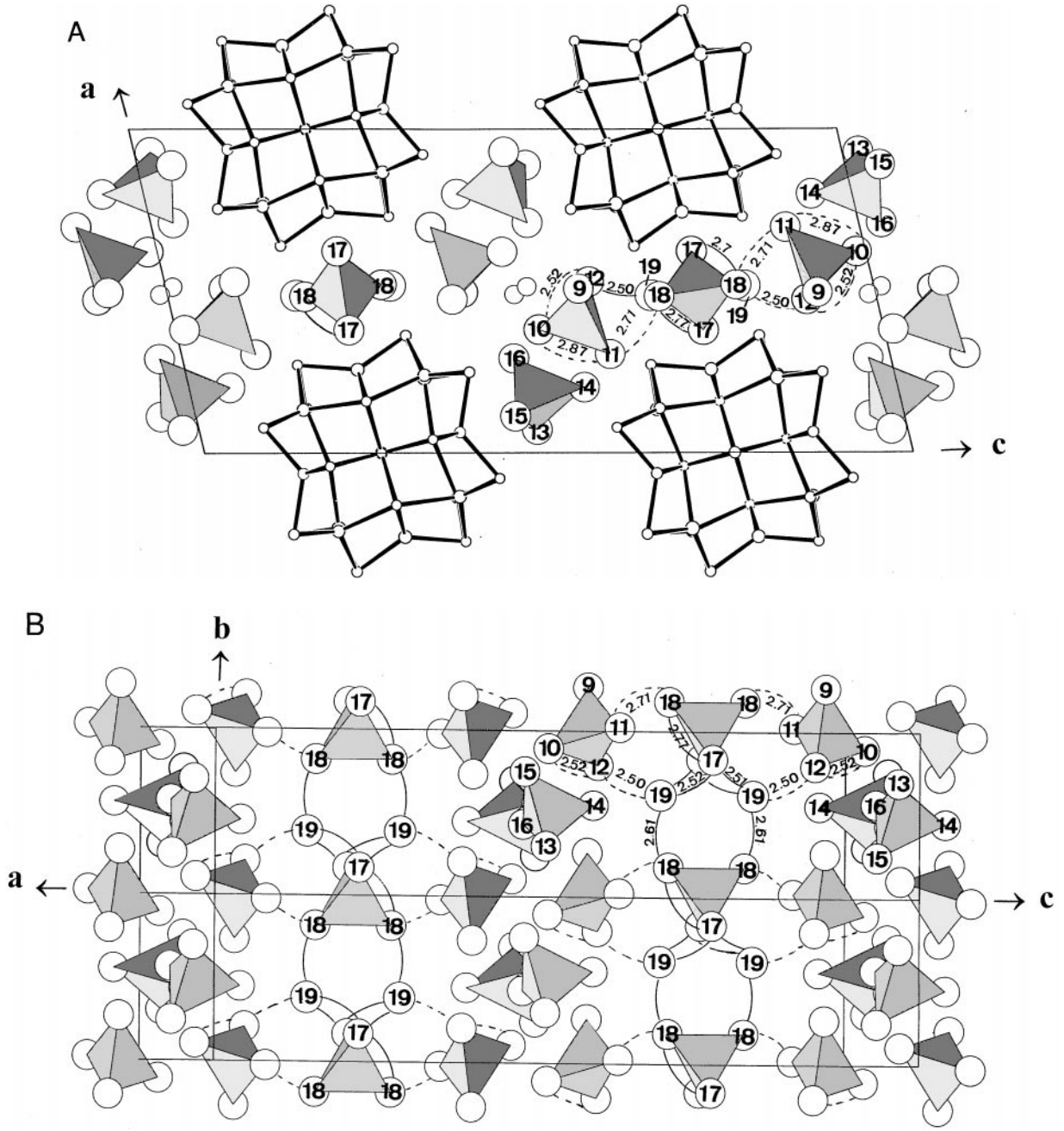

FIG. 7. $Bi_{26}Mo_{9.6}Bi_{0.4}O_{68.4}$ structure with a few O–O distances (a) projection along [0 1 0]; (b) projection along [1 0 0].

ionic conduction layer and favor the oxide anion mobility, as evidenced by numerous experimental techniques.

— $Bi_{26}Mo_{10}O_{69}$ is the first example of a *monodimensional bismuth-based oxide ion conductor*. Beyond the controversy regarding the actual stoichiometry of this new family, the common observed structural characteristics obtained by the different groups of authors exhibit striking similarities with those of the bidimensional compounds described above, especially the BIMEVOX: (i) two types of O atoms are distinguished: those of the $[Bi_{12}O_{14}]_\infty$ columns characterized by short Bi–O bond lengths and low *B* values, and the others, with high *B* values. (ii) Hybridized $6s^2$ lone pairs of the Bi cations (located at the outer side of the columns) are directed toward the O atoms exhibiting high *B* values.

All these observations favor oxide ion mobility involving the O atoms of the Mo surroundings, as the O atoms of the V surroundings are involved in the BIMEVOX compounds; the $[Bi_{12}O_{14}]_\infty$ columns play the same role as the $[Bi_2O_2]$ sheets in the BIMEVOX.

To conclude, our neutron powder diffraction study confirms the existence of two types of oxygen atoms in these compounds: those of the $[Bi_{12}O_{14}]_\infty$ columns and those of the Mo surroundings, these latter likely responsible for the oxide anionic conductivity exhibited by this family of compounds. Measurements of ionic transference number and of resistivity under variable oxygen pressure clearly indicate that these materials can be considered as pure oxide ionic conductors, with negligible electronic semiconduction contribution within the explored temperature and pressure ranges.

ACKNOWLEDGMENTS

We are grateful to Dr. Michel Anne of the Laboratoire de Cristallographie de Grenoble for his advice and to Dr. Jacques Fouletier of LEPMI at Grenoble for conductivity measurements under oxygen partial pressure. The Institut Laue Langevin is thanked for providing neutron facilities and Dr. Emmanuelle Suard (Institut Laue Langevin) is gratefully acknowledged for useful discussions and for her help in the neutron diffraction experiments.

REFERENCES

1. R. N. Vannier, G. Mairesse, F. Abraham, and G. Nowogrocki, *J. Solid State Chem.* **122,** 394 (1996).
2. D. J. Buttrey, T. Vogt, G. P. A. Yap, and A. L. Rheingold, *Mater. Res. Bull.* **32**(7), 947 (1997).
3. R. Enjalbert, G. Hasselmann, and J. Galy, *Acta Crystallogr. C* **53,** 269–272 (1997).
4. R. Enjalbert, G. Hasselmann, and J. Galy, *J. Solid State Chem.* **131,** 236 (1997).
5. C. D. Ling, R. L. Withers, S. Schmid, and J. G. Thompson, *J. Solid State Chem.* **137,** 42–61 (1998).
6. S. C. Abrahams, P. B. Jamieson, and J. L. Bernstein, *J. Chem. Phys.* **47,** 4034, (1967).
7. S. F. Radaev, L. A. Muradyan, and V. I. Simonov, *Acta Crystallogr. Sec. B* **47,** 1, (1991).
8. T. A. Mary, R. Mackay, P. Nguyen, and A. W. Sleight, *Eur. J. Solid State Inorg. Chem.* **33**(4), 285 (1996).
9. J. C. Champarnaud-Mesjard and B. Frit, personal communication.
10. S. Lazure, R. N. Vannier, G. Nowogrocki, G. Mairesse, C. Muller, M. Anne, and P. Strobel, *J. Mater. Chem.* **5**(9), 1395 (1995).
11. C. K. Lee, D. C. Sinclair, and A. R. West, *Solid State Ion.* **62,** 193–198 (1993).
12. L. Hoffart, U. Heider, L. Jörissen, R. A. Huggins, and W. Witschel, *Solid State Ion.* **72,** 195 (1994).
13. T. Esaka, T. Mina-ai, and H. Iwahara, *Solid State Ion.* **52,** 319, (1992).
14. T. Esaka, R. Tachibana, and S. Takai, *Solid State Ion.* **92,** 129 (1996).
15. J. Rodriguez-Carvajal, Fullprof program, version 3.2, Jan. 97.
16. D. J. Buttrey, D. A. Jefferson, and J. M. Thomas, *Philos. Mag. A* **53**(6), 897 (1986).
17. D. J. Buttrey, T. Vogt, U. Wildgruber, and W. R. Robinson, *J. Solid State Chem.* **111,** 118 (1994).
18. I. D. Brown and D. Altermatt, *Acta Crystallogr. Sect. B* **41,** 244 (1985).
19. P. Aldebert, A. J. Dianoux, *J. Phys.* **40,** 1005 (1979).
20. B. E. F. Fender, *in* "Chemical Applications of Thermal Neutron Scattering" (B. T. M. Willis, Ed.), pp. 250–270. Oxford Univ. Press, London, 1974.
21. P. Shuk, H. D. Wiemhöfer, U. Guth, W. Göpel, and M. Greenblatt, *Solid State Ion.* **89,** 179–196 (1996) (and references therein).
22. A. M. Azad, S. Laroze, and S. A. Akbar, *J. Mater. Sci.* **29,** 4135–4151 (1994) (and references therein).
23. F. Honnart, J. C. Boivin, D. Thomas, and K. J. De Vries, *Solid State Ion.* **9–10,** 921 (1983).
24. T. Graia, P. Conflant, J. C. Boivin, and D. Thomas, *Solid State Ion.* **18–19,** 751 (1986).
25. N. M. Sammes, R. J. Philips, and M. G. Fee, *Solid State Ion.* **69,** 121 (1994).
26. P. Conflant, J. C. Boivin, and D. Thomas, *J. Solid State Chem.* **35,** 192 (1980).
27. D. Mercurio, M. El Farissi, J. C. Champarnaud-Mesjard, B. Frit, P. Conflant, and G. Roult, *J. Solid State Chem.* **80,** 133 (1989).
28. D. Mercurio, J. C. Champarnaud-Mesjard, B. Frit, P. Conflant, J. C. Boivin, and T. Vogt, *J. Solid State Chem.* **112,** 1 (1994).
29. K. R. Kendall, C. Navas, J. K. Thomas, and H. C. zur Loye, *Chem. Mater.* **8,** 642–649 (1996).
30. S. Lazure, C. Vernochet, R. N. Vannier, G. Nowogrocki, and G. Mairesse, *Solid State Ion.* **90,** 117–123 (1996).
31. G. Mairesse, *in* Fast Ion Transport in Solids (B. Scrosati Ed.), p. 271. Kluwer, Dordrecht, 1993 (and references therein).
32. I. Abrahams, F. Krok, and J. A. G. Nelstrop, *Solid State Ion.* **90,** 57–65 (1996).
33. I. Abrahams, J. A. G. Nelstrop, F. Krok, and W. Bogusz, *Solid State Ion.* **110,** 95–101 (1998).
34. Y. L. Yang, L. Qiu, W. T. A. Harrison, R. Christoffersen, and A. J. Jacobson, *J. Mater. Chem.* **7**(2), 243–248 (1997).
35. N. Baux, R. N. Vannier, G. Mairesse, and G. Nowogrocki, *Solid State Ion.* **91,** 243–248 (1996).
36. M. S. Islam, S. Lazure, R. N. Vannier, G. Nowogrocki, and G. Mairesse, *J. Mater. Chem.* **8**(3), 655–660 (1998).
37. A. Q. Pham, M. Puri, J. F. Dicarlo, and A. J. Jacobson, *Solid State Ion.* **72,** 309 (1994).
38. K. R. Kendall, J. K. Thomas, and H. C. Zur Loye, *Solid State Ion.* **70/71,** 221 (1994).